THE JOURNAL OF PHYSICAL CHEMISTRY B

Article

pubs.acs.org/JPCB

Structural Dynamics of Al_2O_3/NiAl(110) During Film Growth in NO_2

Rik V. Mom,[†] Joost Vermeer,[†] Joost W.M. Frenken,[†,‡] and Irene M.N Groot*[,†,§]

[†]Huygens-Kamerlingh Onnes Laboratory, Niels Bohrweg 2, 2333 CA Leiden, The Netherlands

[‡]Advanced Research Center for Nanolithography, Science Park 110, 1098 XG Amsterdam, The Netherlands

[§]Leiden Institute of Chemistry, Einsteinweg 55, 2333 CC Leiden, The Netherlands

ABSTRACT: While continuum descriptions of oxide film growth are well established, the local structural dynamics during oxide growth are largely unexplored. Here, we investigate this using scanning tunneling microscopy (STM) and X-ray photoelectron spectroscopy (XPS) for the example of alumina film growth on NiAl(110) following NO_2 exposure. To maintain a well-defined system, we have adopted a cyclic growth approach of NO_2 adsorption and annealing. NO_2 adsorption at 693 K results in the formation of a vacancy island pattern in the NiAl(110) substrate, which is filled with AlO_x by diffusion of O through the alumina film. The patches of AlO_x coalesce to form smooth terraces upon annealing to 1200 K. By repeated cycling, we have grown films of up to 0.9 nm thick. While peak shifts in the XPS spectra indicate that the film maintains its insulating character upon thickening, our STM data show that there is a finite density of states within the band gap. The thickening of the alumina film is accompanied by the formation of trenches in the surface, which we interpret to be the result of film stress relief.

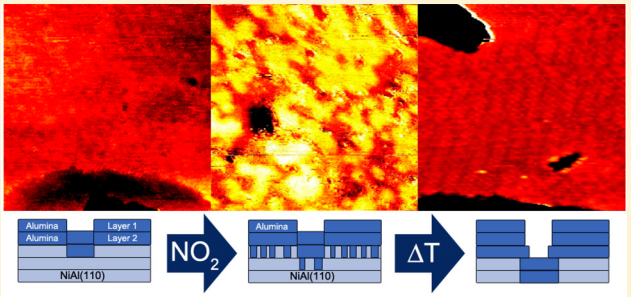

INTRODUCTION

Oxide films find wide use as a result of both their chemical and electrical properties. Some oxide films, such as IrO_2, provide extraordinary catalytic activity, while others, such as Al_2O_3, are employed mainly because of their chemical inertness. Efficient electrical insulation can be provided by nanoscale oxide layers, such as SiO_2 and HfO_2. In all of these applications, control over the layer thickness, the structure, and the stability of the oxide films is essential. Therefore, the growth mechanisms of oxide films have been the subject of intense investigation for decades.

Phenomenologically, oxide film growth by oxidation of a metal substrate is described well by the Cabrera-Mott model[1,2] for thin films (<20 nm) and the Wagner model[3,4] for thicker films. In both models, the initial step is the adsorption of the oxidant (O_2 for instance) on the oxide layer. Subsequently, electrons are transferred from the metal substrate to the adsorbed oxygen atoms or molecules. For thin films, this process occurs primarily via tunneling and results in the formation of an electric field (the Mott potential). This field provides a driving force for the diffusion of ions, thus allowing for oxide film growth at relatively mild temperatures. However, the field strength decays as the film thickens. Hence, for thicker films ion diffusion is a mere thermal process as described in Wagner's model.

While the Cabrera-Mott and Wagner models provide a meaningful generic picture of the most essential processes underlying oxide film growth, many system-specific properties are not taken into account. For instance, the atomic and electronic structure of the oxide often changes as a function of film thickness.[5−8] As a result of this, the adsorption of oxidant molecules may also show a thickness dependence.[5] Furthermore, the oxide film may not grow in a uniform layer-by-layer fashion as implicitly assumed by continuum models. Thus, surface roughness may develop.

From the examples mentioned above, it should be clear that detailed knowledge of the atomic-scale processes on oxide films is required for a full understanding of oxide film growth. Crystalline oxide films grown on metal single crystals provide an excellent platform to gain such detailed insight. Because of its technological importance, alumina has been one of the main subjects of these model studies. A range of crystalline alumina films can be prepared on nickel−aluminum single crystals.[9−13] The rates of film growth in oxidants, such as O_2, H_2O, and NO_2, vary strongly for these films.[6,10−17] In particular, the films with unsaturated aluminum surface sites[13] or structural disorder[13,15] are reactive, as they readily adsorb molecules from the gas phase. The alumina film on NiAl(110) is among the least reactive, which can be attributed to its dense packing of oxygen atoms at the surface.[18] Under ultrahigh vacuum (UHV) conditions, film growth using O_2 could only be achieved on this surface at temperatures above 770 K.[19] Furthermore, the surface could not be hydrated by H_2O exposure at room temperature.[6] However, H_2O dissociation on defect sites at low temperatures provides a growth mechanism during repeated H_2O-exposure and temperature-programmed desorption (TPD) runs.[17] The reactivity toward NO_2 is much

Special Issue: Miquel B. Salmeron Festschrift

Received: July 11, 2017
Revised: October 10, 2017
Published: October 17, 2017

DOI: 10.1021/acs.jpcb.7b06790
J. Phys. Chem. B 2018, 122, 788−793

higher, allowing for substantial film growth at room temperature in UHV.[16]

While the studies mentioned above have given detailed information on the reactivity of alumina films, the experimental evidence was nearly exclusively obtained from laterally averaging techniques, in particular from TPD, X-ray photoelectron spectroscopy (XPS), and low-energy electron diffraction (LEED). Thus, little is known about local structural variations and surface roughness evolution during film growth, which can provide important insights into the individual steps in the film growth process.

To follow the local surface structure during oxide film growth, we have used scanning tunneling microscopy (STM) to study the structural evolution of Al_2O_3/NiAl(110) resulting from NO_2 exposure. By employing a cyclic adsorption-annealing procedure, we have maintained the crystallinity of the oxide layer, thus assisting the identification of the observed structures with atomic-level detail.

METHODS

The experiments were carried out in a home-built UHV system described in detail previously.[20−22] The system consists of a preparation chamber with a corrosion-resistant turbomolecular pump, an XPS chamber equipped with a commercial SPECS Phoibos electron analyzer and a monochromated X-ray source (Al anode) and an STM chamber with a home-built STM system, run via in-house developed electronics.

The NiAl(110) specimen (purchased from Surface Preparation Laboratory)[23] was cleaned in situ by cycles of 1.5 keV Ar^+ sputtering and annealing at 1300 K. The initial alumina layer was formed by three cycles of 5×10^{-6} mbar O_2 exposure at 550 K and subsequent UHV annealing at 1100 K (1050 K in the final cycle).[9] The cleanliness and crystalline quality of the surface were checked by XPS and STM before further use. NO_2 (Sigma-Aldrich >99.5% purity) was dosed via backfilling of the preparation chamber.

In the XPS experiments, the X-ray incidence angle was set at 54° off normal, while the photoelectrons were collected along the surface normal. The spectra were analyzed using the CasaXPS software package.[24] For the Al 2p/Ni 2p region, a linear background subtraction was applied, while a Shirley background subtraction was used for the O 1s spectra. The energy scale was calibrated using the Al^0 2p and O 1s peaks of the initial alumina film (before NO_2 exposure), in accordance with literature values.[14,16] Peak fitting was performed using the standard Gaussian/Lorentzian curves implemented in CasaXPS. The Al 2p/Ni 2p region was fitted using three doublets. While it is known that this region in fact consists of four contributions,[14,16] the two Al^{3+} contributions (surface and oxide-metal interface species) could not be resolved individually using our lab source. Each p-doublet was forced to obey the 3:2 intensity ratio, appropriate for a spin−orbit split p-to-continuum transition. Furthermore, the full widths at half-maximum of the two peaks in every doublet were set equal to each other.

The oxide film thickness can be calculated both from the Al^{3+}/Al^0 2p ratio and the O 1s/Ni 2p ratio:[25]

$$d = \lambda_{Al^{3+}} \sin(\theta) \ln\left(\frac{\alpha I_{Al^{3+}}}{I_{Al^0}} + 1\right) \quad (1)$$

$$\frac{I_{O1s}}{I_{Ni2p}} = \beta \frac{1 - e^{-d/\lambda_o}}{e^{-d/\lambda_{Ni}}} \quad (2)$$

In eqs 1 and 2, d is the film thickness, λ_i is the effective attenuation length for electrons originating from species i, θ is angle between the analyzer and the surface normal, I_i is the measured XPS peak area for species i, and α and β are proportionality factors taking into account sensitivity and geometrical factors. The proportionality constants were calibrated using the spectra of the initial as-prepared alumina film, which is known to be 0.5 nm thick.[18] For λ_{Al3+}, λ_O and λ_{Ni}, we found[26] 2.85, 2.04, and 2.88 nm respectively, based on the known structure of the alumina film.[18] To enable a comparison to the results from Staudt et al.,[16] we calculated the oxide film thickness from the I_{Al3+}/I_{Al0} ratio given in their work using eq 1, with λ_{Al3+} = 0.305 nm (note that this was synchrotron data recorded with 150 eV incidence energy, resulting in a much lower value for λ_{Al3+}).

The STM measurements were carried out in vacuum at room temperature. Cut $Pt_{0.8}Ir_{0.2}$ wire (ø 0.25 mm, Goodfellow) was used as the tip material. The images were recorded and analyzed using the Camera 4.3 software, developed in-house.

RESULTS

NO_2 Exposure at 693 K. To investigate the structural evolution of the oxide film during NO_2 adsorption, we exposed an alumina film that had been prepared using O_2 to 5×10^{-7} mbar NO_2 for 5 min at 693 K and subsequently imaged the sample using STM at room temperature. Figure 1a shows the initial alumina film. Wide terraces are observed, on which the signature of the atomic structure of the Al_2O_3/NiAl(110)

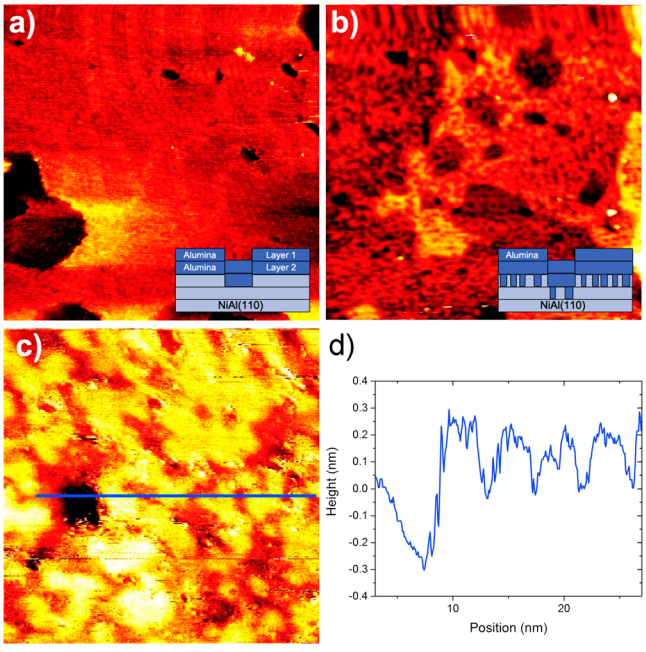

Figure 1. Morphology changes on Al_2O_3/NiAl(110) following a 5 min exposure to 5×10^{-7} mbar NO_2 at 693 K. (a) As prepared sample. 80 × 80 nm^2, U_s = −1.5 V, I_t = 105 pA. (b) Sample after exposure to NO_2. 160 × 160 nm^2, U_s = −1 V, I_t = 55 pA. (c) Same as (b), 31 × 31 nm^2, U_s = −1 V, I_t = 55 pA. The blue line indicates the location of the height line displayed in (d). The insets in (a) and (b) show a model of the distribution of alumina in the system, based on the discussion in this section.

DOI: 10.1021/acs.jpcb.7b06790
J. Phys. Chem. B 2018, 122, 788−793

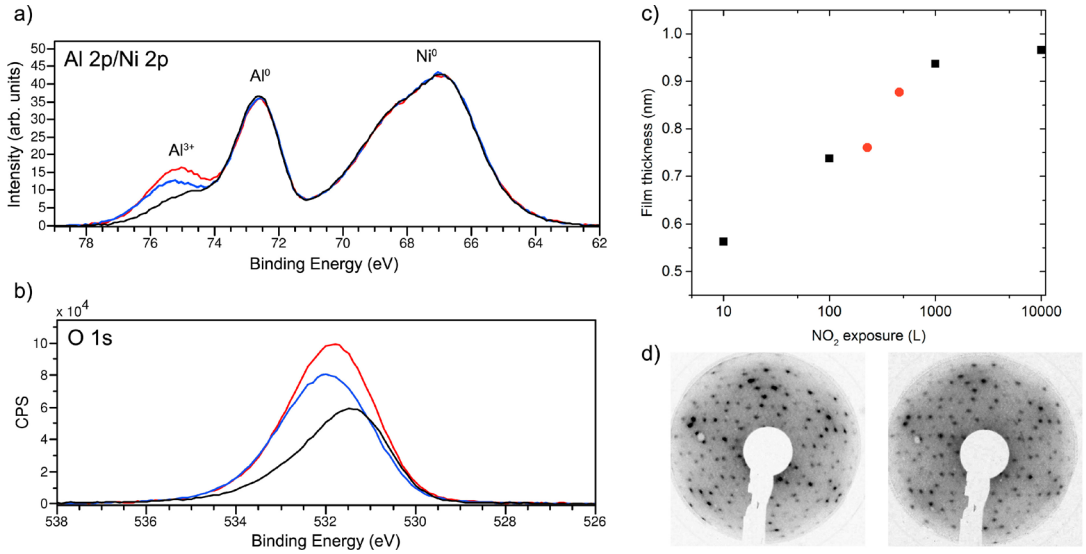

Figure 2. XPS spectra recorded after cycles of NO_2 adsorption at 693 K and annealing at 1200 K. (a) Al 2p/Ni 2p spectra of the as-prepared film (black), after 2 cycles (blue) and after 4 cycles (red). The spectra are shown after background subtraction and normalization to Ni 2p peak for easy comparison. (b) Corresponding O 1s spectra, shown after background subtraction, without normalization. (c) Film thickness as a function of exposure, calculated using eq 1 (red circles). The data are compared to calculations based on room temperature NO_2 exposure data from Staudt et al.[16] (black squares). (d) LEED patterns of an as-prepared film (left) and after 3 oxidation cycles (right).

surface can be recognized. The film shows some vacancy islands, in which the same film structure is recognized, indicating that the alumina film also has the well-characterized[18] two-layer structure here. Hence, the vacancy islands are locations where the metal NiAl(110) substrate has a vacancy island rather than the alumina film (see inset of Figure 1a). For the interpretation of morphological changes that occur upon NO_2 adsorption, it is important to consider the insulating character of the alumina film, and its appearance in STM. Due to the band gap of the aluminum oxide film, almost no tunneling occurs from the film to the tip at the sample bias employed here.[27,28] Hence, the tunneling current signal predominantly reflects the tunneling behavior of the NiAl(110) substrate. The presence of the alumina film likely lowers the tunneling barrier. The extent to which the barrier is lowered varies locally, allowing one to observe the atomic structure of the alumina film.[18]

With this picture in mind, we can interpret the morphology changes in the sample following NO_2 adsorption, shown in Figures 1b–d. The terraces observed on the as-prepared film appear to break up into a finer-scale two-level pattern. As NO_2 decomposes completely at the employed temperature,[16] one can exclude the formation of an $Al(NO_x)_y$ compound as a cause for this behavior. The height difference between the levels is 0.19 nm, which is very close to the step height measured on the as-prepared alumina film (0.21 nm). In the latter case, the measured step height reflects the monatomic step height of the NiAl(110) substrate, since the film is two alumina layers thick over the entire surface (see inset of Figure 1a). Hence, the observation that the two-level pattern has the same height implies that vacancy islands have been formed in the NiAl(110) substrate. Consistent with this, two-level patterns as observed in Figure 1 are typical for surface etching in combination with limited diffusion.[29,30]

The observation of vacancy islands in the NiAl(110) substrate indicates that metallic Al has been oxidized. Indeed, Staudt et al. observed an increase in the Al^{3+} contribution in their XPS spectra, even when dosing NO_2 at room temperature.[16] The vacancy islands could either be voids between NiAl(110) and the alumina film, or areas where Al has been replaced by AlO_x, which is invisible to STM. The exsistence of voids seems unlikely in this case, as it implies a large amount of dangling bonds. Given the intimate binding between the NiAl(110) substrate and the alumina film,[18] this appears energetically unfavorable. Moreover, voids usually adopt a (near) spherical shape to minimize the amount of dangling bonds. In the present case, the vacancy islands are only a single layer deep.

The Al oxidation is followed by diffusion of either Al cations or oxygen anions through the film to form a new oxide layer. In the case of cation diffusion, the new oxide layer will be formed on top of the oxide film. In contrast, anion diffusion will result in oxide growth at the $NiAl/Al_2O_3$ interface. Which of these scenarios prevails is system-dependent.[31] In the oxidation studies on Al_2O_3/NiAl(110), it is sometimes assumed that Al^{3+} diffuses to the surface.[14,32] However, this assumption seems incompatible with the fine etching pattern observed here. If the Al^{3+} ions formed during oxidation of the NiAl substrate diffuse through the film, the preexisting alumina film would have to be broken up in order to fill the vacancies that the Al^{3+} ions leave behind. For a fine vacancy island pattern observed here, this would involve a significant amount of bond breaking. Thus, we suggest that it is not Al^{3+}, but O^{2-} that diffuses through the alumina film, filling the vacancy islands in the NiAl(110) substrate with AlO_x.

In the situation described above, where the new oxide grows at the oxide-metal interface, the physical height of the sample changes little. When Al from the substrate is converted to nonconductive AlO_x at the same location, a vacancy island will be observed in STM, even though the topographic height of the surface has remained equal or is even slightly higher. The presence of the alumina film only affects the tunneling barrier. This effect is stronger at locations where the film has three layers rather than two. This could explain why the observed step height (0.19 nm) is slightly less than the NiAl(110) step height (0.21 nm).

DOI: 10.1021/acs.jpcb.7b06790
J. Phys. Chem. B 2018, 122, 788–793

A more detailed inspection of Figure 1b and c shows that the two-level pattern is homogeneous over the surface, without alterations around the step edges of the substrate. This implies that NO_2 adsorption and the subsequent oxidation of the NiAl substrate have no preference for step edges. Based on the densily packed oxygen termination of the perfect alumina film,[18] this is a surprising finding. One may speculate that the defects on the oxide film's terraces play an important role in facilitating the NO_2 adsorption. For metal adsorption on the alumina film, it was shown that these defects bind significantly stronger than the perfect terrace sites.[33]

Summarizing, we suggest the following oxidation mechanism. (1) Metallic Al at the NiAl(110)-alumina interface is oxidized. (2) Oxygen anions diffuse through the alumina film, forming a AlO_x nucleus at the NiAl-alumina interface. (3) The AlO_x nuclei coalesce into islands. As these islands replace the metallic Al that was initially present at the NiAl-alumina interface, they appear as vacancy islands in the STM images.

Adsorption-Annealing Cycled Growth. To investigate the dependence of the film growth properties on film thickness, while maintaining a crystalline oxide film, we adopted a cycled growth strategy. Every cycle consists of NO_2 adsorption at a pressure of 5×10^{-7} mbar and a temperature of 693 K for 5 min, followed by annealing in UHV at 1200 K for 7 min. Figure 2 shows XPS data obtained using this approach. As expected, a clear rise in the Al^{3+}/Al^0 ratio is apparent in the Al 2p/Ni 2p spectra following oxidation cycling, indicating film growth. Concomitantly, the O 1s peak rises. Using the spectral decomposition described in the Methods Section, the Al^{3+} 2p, Al^0 2p, and Ni 2p contributions were quantified and compared to the O 1s intensity. The Al^0 2p/Ni 2p peak area ratio is unaffected by the treatment, showing that the annealing step suffices to replenish the oxidized Al at the oxide-metal interface. Furthermore, no nitrogen was detected, indicating that the film is fully oxidic. Finally, the O 1s/Al^{3+} 2p ratio remains constant, hence there is also no change in stoichiometry in the oxide film. This is in agreement with the observation here and in the literature that the LEED pattern remains constant (see Figure 2d) for films with a thickness up to at least 1.4 nm.[34,35]

The film thickness calculated using the Al^{3+}/Al^0 2p ratio yielded results equal to those obtained from the O 1s/Ni 2p ratio, indicating that the spectral decomposition of the Al^{3+} and Al^0 components was accurate. Figure 2c compares the film growth rate obtained in the present study to data from Staudt et al., who exposed their sample at room temperature. Remarkably, the calculated growth rates are very comparable, even though in the present case we have dosed NO_2 at much higher temperature. Two causes can be identified for this. First, at room temperature the Al^0 concentration in the near-surface region will be depleted, as transport from the bulk is slow at mild temperatures.[14] Since eq 1 does not take this into account, the calculated film thickness is an overestimation. Nonetheless, we point out that the depletion of Al even at the oxide-metal interface was not high enough to prevent further film growth in the compared region. A second reason could be that the film crystallinity deteriorated in the room temperature experiment. Such a defective oxide may facilitate easier adsorption and ion diffusion. In addition to these two causes one could imagine that oxygen is lost from the alumina substrate during the annealing step. However, we established that additional annealing does not lead to a loss of oxygen.

Following the NO_2 treatment, both the O 1s and Al^{3+} 2p peaks shift to higher binding energies. This can be understood as follows. The core holes created in the alumina film during photoionization cannot be screened by the film itself, due to its insulating character. For thin films, partial hole screening is nonetheless accomplished by the NiAl substrate. As the film grows, this mechanism becomes less effective, resulting in an interaction between the departing photoelectron and the core hole that stays behind. Thus, the photoelectron will be emitted from the surface with a reduced kinetic energy, resulting in a higher apparent binding energy. After 4 oxidation cycles, the O 1s and Al^{3+} 2p peaks shift slightly back. This could be due to an increase in the number of defects in the film, which increases the density of states in the band gap, effectively increasing the film's conductivity. Corroborating this, Staudt et al. observed much smaller peak shifts after dosing NO_2 at room temperature (highly defective film).[16] Upon subsequent annealing (crystallization) the peak shifts increased.

Figure 3a shows the film morphology after two complete adsorption-annealing cycles of NO_2 treatment. Clearly, the

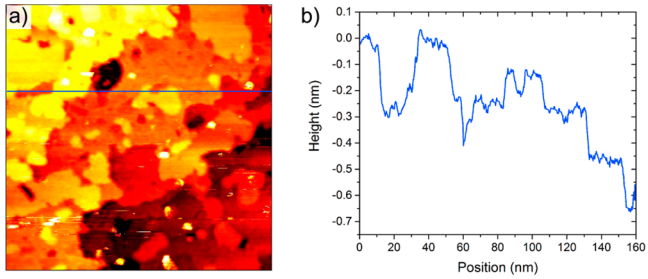

Figure 3. STM image of the alumina film after 2 cycles of NO_2 adsorption/annealing. (a) 160×160 nm^2 image, with $U_s = -1$ V, $I_t = 100$ pA. The blue line in the image indicates the location of the height line shown in (b).

annealing results in sintering of the vacancy islands that were observed in Figure 1, rendering smoother terraces. Nonetheless, the density of islands and vacancy islands is much larger than that of the initial two-layer film. Analysis of the observed step heights shows that single steps in the NiAl(110) substrate are no longer dominant. The height line in Figure 3b exemplifies this, showing step heights of 0.15 and 0.3 nm. Only vaguely visible in Figure 3, vacancy islands with a step height of less than 0.1 nm are observed. Such steps are smaller than monatomic height. This implies that there are either multiple Ni_xAl_y phases present at the metal-oxide interface, or that the oxide film itself affects the tunneling current. Since the XPS and LEED data indicate no change in the film and interface structure, we interpret the observed step heights as due to the alumina film.

The alumina film can affect the tunneling signal in two ways. As pointed out in NO_2 Exposure at 693 K Section, the film reduces the (average) tunneling barrier, with an extend that depends on the film thickness. Local variations in film thickness may therefore affect the apparent height observed in STM images. Second, electrons may tunnel from the alumina film itself. For the initial, high quality two layer film, the tunneling electrons predominantly originate from the NiAl substrate. As the film thickens, the STM tip will have to move closer to the alumina surface in order to obtain the desired tunneling current. As the tunneling probability has an exponential dependence on the tip−sample distance, even a very low

DOI: 10.1021/acs.jpcb.7b06790
J. Phys. Chem. B 2018, 122, 788−793

density of states around the Fermi level in the oxide will cause a significant tunneling current. Thus, if there is a finite density of states in the band gap of the alumina film, it will become visible in STM.

In NO_2 Exposure at 693 K Section we observed that a change in tunneling barrier due to a variation of 1 layer of alumina only has a minor effect on the observed NiAl(110) step height (0.19 nm versus 0.21 nm). Therefore, this mechanism cannot be the sole explanation for the behavior observed in Figure 3. Thus, we conclude that the alumina film contributes to the tunneling current, implying that it is not a pure insulator, but rather contains a finite density of gap states.

Figure 4 shows the film morphology after 3 oxidation cycles. While the number of small islands appears to have decreased,

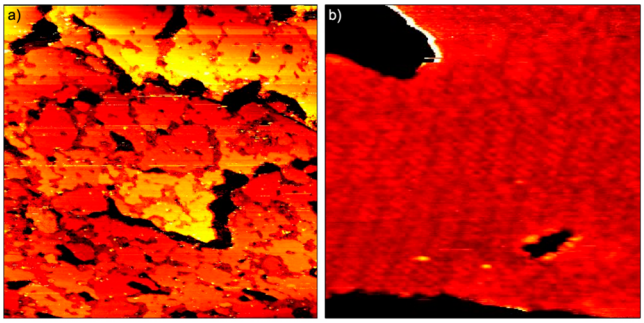

Figure 4. Alumina film after 3 cycles of NO_2 adsorption/annealing. (a) 320 × 320 nm^2 image, with U_s = −1 V, I_t = 105 pA. (b) Higher-resolution image, showing the film's crystallinity. Size: 25 × 25 nm^2, U_s = −1.5 V, I_t = 40 pA.

trenches develop in the surface. The depth of these trenches often exceeds 1 nm. This indicates that these are genuine trenches in the surface, rather than local regions of extra thick oxide film (the STM tip would have crashed into the surface at these "trenches" otherwise). Thus, the NiAl substrate has not only been etched in the trenches, but Al^{3+} diffusion must have occurred too in order to relocate the oxide film. This is in contrast to the first stages of film growth at 693 K, in which all vacancy islands in the NiAl substrate were filled with oxide. We interpret this striking observation as follows. First, we note that the structure of the alumina film is not that of a bulk alumina phase. This is due to the interaction with the substrate, which forces the alumina film to adopt a structure that slightly deviates from the ideal. Hence, as the film grows thicker, stress builds up, both in the alumina film itself and in the top layers of the NiAl substrate. Discontinuities such as steps and trenches relieve this stress. Trenches are particularly favorable, as they are able to relieve stress also in deeper layers. Thus, there is a thermodynamic driving force for the formation of trenches, which takes place even though the serrated step edge morphology of the surface shows that the surface is not able to equilibrate fully.

Finally, we discuss the possible applications of the thickened alumina film. As shown in Figure 4, the film maintains a high degree of crystalline order, even at the level of scrutiny of STM. This makes the thicker alumina films suitable as substrates for well-defined surface-science studies. Al_2O_3/NiAl(110) with a film thickness of 0.5 nm has been widely used as a substrate for model nanoparticle catalysts.[28,36−38] However, charge transfer between the nanoparticles and the metal substrate is commonly observed when using such ultrathin films,[39,40] possibly causing these model catalysts to behave differently from their industrial counterparts. The use of thicker alumina films could reduce these differences. One might also imagine a higher chemical stability for the thicker alumina films. For the 0.5 nm film, nanoparticles catalyze oxide film growth in O_2,[37,38,41] rendering the film sensitive at room temperature even to UHV exposures. For the example of MoO_3 nanoparticles, we have established that this catalytic mechanism remains active even in case of the thickened alumina films. Thus, the thicker films do not provide a sufficient barrier to guarantee full chemical stability.

Apart from its use in catalysis, the Al_2O_3/NiAl(110) system has also been discussed as a model system for metal−insulator−metal devices[35,42] and nanoelectronics.[32] In such cases, the most essential properties are the film's insulating characteristics. The shifts in our XPS peaks clearly establish that the insulating character of the alumina film is maintained upon thickening. However, our STM data suggest that the film exhibits a finite density of electronic states within the band gap, which should be interpreted as an imperfection in the insulating character. Furthermore, the thicker films do not have a uniform thickness, which could be detrimental to the tunneling properties for metal−insulator−metal devices. Thus, while the film could serve as a good model for a realistic device, the behavior will likely not be ideal.

CONCLUSION

We have used STM to explore the local structural rearrangements of Al_2O_3 on NiAl(110) upon NO_2 exposure. NO_2 adsorption at 693 K makes the alumina grow at the oxide-metal interface, consuming metallic Al in the process. Due to diffusion limitations, this results in a fine etching pattern where patches of alumina and NiAl of a few nanometer in size are mixed. Annealing at 1200 K allows for island coalescence, yielding smooth terraces. Under these conditions, the metallic Al at the oxide-metal interface is replenished.

To examine the film growth properties at various film thicknesses, while maintaining a well-defined character in the alumina film, we adopted a cyclic growth method. Each cycle consisted of NO_2 adsorption for 5 min at 5 × 10^{-7} mbar and 693 K, followed by annealing at 1200 K for 7 min. Observations by LEED and STM, and XPS measurements of the O/Al stoichiometry indicate that the crystal structure of the alumina film is maintained during the cycled film growth in the investigated thickness range (0.5 to 0.9 nm). The large-scale morphology is modified, however, showing a decrease in terrace size. After 3 oxidation cycles, the development of trenches is evident. We interpret this as the result of stress relief. Such stress is built up as the film thickens because the film−substrate interaction forces the alumina film to maintain a structure that deviates from that of bulk alumina phases.

Our XPS results indicate that the alumina film maintains an insulating character during film growth. However, our STM data show that some, possibly very low density of states must be present in the band gap.

AUTHOR INFORMATION

Corresponding Author

*i.m.n.groot@lic.leidenuniv.nl.

ORCID

Irene M.N Groot: 0000-0001-9747-3522

Notes

The authors declare no competing financial interest.

DOI: 10.1021/acs.jpcb.7b06790
J. Phys. Chem. B 2018, 122, 788−793

REFERENCES

(1) Cabrera, N.; Mott, N. F. Theory of the Oxidation of Metals. *Rep. Prog. Phys.* **1949**, *12*, 163−184.
(2) Xu, Z.; Rosso, K. M.; Bruemmer, S. Metal Oxidation Kinetics and the Transition from Thin to Thick Films. *Phys. Chem. Chem. Phys.* **2012**, *14*, 14534−14539.
(3) Wagner, C. The Theory of the Warm-up Process. *Z. Phys. Chem.* **1933**, *21B*, 25−41.
(4) Atkinson, A. Transport Processes during the Growth of Oxide Film at Elevated Temperature. *Rev. Mod. Phys.* **1985**, *57*, 437−470.
(5) Baran, J. D.; Grönbeck, H.; Hellman, A. Mechanism for Limiting Thickness of Thin Oxide Films on Aluminum. *Phys. Rev. Lett.* **2014**, *112*, 146103.
(6) Freund, H.-J. Introductory Lecture: Oxide Surfaces. *Faraday Discuss.* **1999**, *114*, 1−31.
(7) Freund, H.-J.; Pacchioni, G. Oxide Ultra-Thin Films on Metals: New Materials for the Design of Supported Metal Catalysts. *Chem. Soc. Rev.* **2008**, *37*, 2224−2242.
(8) Shaikhutdinov, S.; Freund, H.-J. Ultrathin Oxide Films on Metal Supports: Structure-Reactivity Relations. *Annu. Rev. Phys. Chem.* **2012**, *63*, 619−633.
(9) Jaeger, R. M.; Kuhlenbeck, H.; Freund, H.; Wuttig, M.; Hoffmann, W.; Franchy, R.; Ibach, H. Formation of a Well-Ordered Aluminium Oxide Overlayer by Oxidation of NiAl (110). *Surf. Sci.* **1991**, *259*, 235−252.
(10) Qin, F.; Magtoto, N. P.; Kelber, J. A. H2O-Induced Instability of Al2O3/Ni 3Al(110) and Al2O3/Ni3Al(111) Thin Films under Non-UHV Conditions. *Surf. Sci.* **2004**, *565*, L277−L282.
(11) Kelber, J. A. Alumina Surfaces and Interfaces under Non-Ultrahigh Vacuum Conditions. *Surf. Sci. Rep.* **2007**, *62*, 271−303.
(12) Ozensoy, E.; Peden, C. H. F.; Szanyi, J. NO2 Adsorption on Ultrathin Theta-Al2O3 Films: Formation of Nitrite and Nitrate Species. *J. Phys. Chem. B* **2005**, *109*, 15977−15984.
(13) Maurice, V.; Frémy, N.; Marcus, P. Hydroxylation-Induced Modifications of the Al2O3/NiAl(001) Surface at Low Water Vapour Pressure. *Surf. Sci.* **2005**, *581*, 88−104.
(14) Shavorskiy, A.; Müller, K.; Newberg, J. T.; Starr, D. E.; Bluhm, H. Hydroxylation of Ultrathin Al2O3 /NiAl(110) Films at Environmental Humidity. *J. Phys. Chem. C* **2014**, *118*, 29340−29349.
(15) Ivey, M. M.; Layman, K. A.; Avoyan, A.; Allen, H. C.; Hemminger, J. C. Characterization of Ultrathin Films of Gamma-Al2O3 and the Chemistry of 1,3-Butadiene on NiAl(001) and Gamma-Al2O3. *J. Phys. Chem. B* **2003**, *107*, 6391−6400.
(16) Staudt, T.; Desikusumastuti, A.; Happel, M.; Vesselli, E.; Baraldi, A.; Gardonio, S.; Lizzit, S.; Rohr, F.; Libuda, J. Modeling NOx Storage Materials: A High-Resolution Photoelectron Spectroscopy Study on the Interaction of NO2 with Al2O3/NiAl(110) and BaO/Al2O3/NiAl(110). *J. Phys. Chem. C* **2008**, *112*, 9835−9846.
(17) Yi, C. W.; Szanyi, J. D2O Adsorption on an Ultrathin Alumina Film on NiAl(110). *J. Phys. Chem. C* **2007**, *111*, 17597−17602.
(18) Kresse, G.; Schmid, M.; Napetschnig, E.; Shishkin, M.; Köhler, L.; Varga, P. Structure of the Ultrathin Aluminum Oxide Film on NiAl(110). *Science (Washington, DC, U. S.)* **2005**, *308*, 1440−1442.
(19) Yoshitake, M.; Lay, T.; Song, W. Well-Ordered Ultra-Thin Al2O3 Film Formation on NiAl(110) by High-Temperature Oxidation. *Surf. Sci.* **2004**, *564*, 211−217.
(20) Herbschleb, C. T.; van der Tuijn, P. C.; Roobol, S. B.; Navarro, V.; Bakker, J. W.; Liu, Q.; Stoltz, D.; Cañas-Ventura, M. E.; Verdoes, G.; van Spronsen, M. A.; et al. The ReactorSTM: Atomically Resolved Scanning Tunneling Microscopy under High-Pressure, High-Temperature Catalytic Reaction Conditions. *Rev. Sci. Instrum.* **2014**, *85*, 083703.
(21) Rost, M. J.; van Baarle, G. J. C.; Katan, A. J.; van Spengen, W. M.; Schakel, P.; van Loo, W. A.; Oosterkamp, T. H.; Frenken, J. W. M. Video-Rate Scanning Probe Control Challenges: Setting the Stage for a Microscopy Revolution. *Asian J. Control* **2009**, *11*, 110−129.
(22) Rost, M. J.; Crama, L.; Schakel, P.; Van Tol, E.; Van Velzen-Williams, G. B. E. M.; Overgauw, C. F.; Ter Horst, H.; Dekker, H.; Okhuijsen, B.; Seynen, M.; et al. Scanning Probe Microscopes Go Video Rate and beyond. *Rev. Sci. Instrum.* **2005**, *76*, 053710.
(23) *Surface Preparation Laboratory* Penningweg 69F, 1507 DE Zaandam, The Netherlands.
(24) Fairley, N. *CasaXPS 2.3*; 1999.
(25) Cumpson, P. J.; Seah, M. P. Elastic Scattering Corrections in AES and XPS. II. Estimating Attenuation Lengths and Conditions Required for Their Valid Use in Overlayer/Substrate Experiments. *Surf. Interface Anal.* **1997**, *25*, 430−446.
(26) Powell, C. J.; Jablonski, A. *NIST Electron Effective-Attenuation-Length Database 1.3*; NIST: Gaitherburg, United States, 2011.
(27) Højrup Hansen, K.; Worren, T.; Lægsgaard, E.; Besenbacher, F.; Stensgaard, I. Bias Dependent Apparent Height of an Al2O3 Thin Film on NiAl(110), and of Supported Pd Clusters. *Surf. Sci.* **2001**, *475*, 96−102.
(28) Napetschnig, E.; Schmid, M.; Varga, P. Pd, Co and Co-Pd Clusters on the Ordered Alumina Film on NiAl(110): Contact Angle, Surface Structure and Composition. *Surf. Sci.* **2007**, *601*, 3233−3245.
(29) Min, B. K.; Alemozafar, A. R.; Biener, M. M.; Biener, J.; Friend, C. M. Reaction of Au(111) with Sulfur and Oxygen: Scanning Tunneling Microscopic Study. *Top. Catal.* **2005**, *36*, 77−90.
(30) Biener, M. M.; Biener, J.; Friend, C. M. Sulfur-Induced Mobilization of Au Surface Atoms on Au (111) Studied by Real-Time STM. *Surf. Sci.* **2007**, *601*, 1659−1667.
(31) Brossmann, U.; Würschum, R.; Södervall, U.; Schaefer, H.-E. Oxygen Diffusion in Ultrafine Grained Monoclinic ZrO2. *J. Appl. Phys.* **1999**, *85*, 7646−7654.
(32) Kelber, J.; Magtoto, N.; Vamala, C.; Jain, M.; Jennison, D. R.; Schultz, P. A. Reactivities of Ultrathin Alumina Films Exposed to Intermediate Pressures of H2O: Substrate-Mediated Mechanism for Growth and Loss of Surface Order. *Surf. Sci.* **2007**, *601*, 3464−3471.
(33) Bäumer, M.; Freund, H.-J. Metal Deposits on Well-Ordered Oxide Films. *Prog. Surf. Sci.* **1999**, *61*, 127−198.
(34) Yoshitake, M.; Mebarki, B.; Lay, T. T. Crystallinity and Thickness Control of Well-Ordered Ultra-Thin Al2O3 Film on NiAl (110). *Surf. Sci.* **2002**, *511*, L313.
(35) Lay, T. T.; Yoshitake, M.; Song, W. Epitaxial Growth of Well-Ordered Ultra-Thin Al2O3 Film on NiAl (110) by a Single-Step Oxidation. *Appl. Surf. Sci.* **2005**, *239*, 451−457.
(36) Bäumer, M.; Frank, M.; Heemeier, M.; Kühnemuth, R.; Stempel, S.; Freund, H.-J. Nucleation and Growth of Transition Metals on a Thin Alumina Film. *Surf. Sci.* **2000**, *456*, 957−962.
(37) Mom, R. V.; Rost, M. J.; Frenken, J. W. M.; Groot, I. M. N. Tuning the Properties of Molybdenum Oxide on Al2O3/NiAl(110): Metal versus Oxide Deposition. *J. Phys. Chem. C* **2016**, *120*, 19737−19743.
(38) Bäumer, M.; Biener, J.; Madix, R. J. Growth, Electronic Properties and Reactivity of Vanadium Deposited onto a Thin Alumina Film. *Surf. Sci.* **1999**, *432*, 189−198.
(39) Netzer, F. P.; Fortunelli, A. *Oxide Materials at the Two-Dimensional Limit*; Springer, 2016.
(40) Zhu, J.; Giordano, L.; Lin, S.; Fang, Z.; Li, Y.; Huang, X.; Zhang, Y.; Pacchioni, G. Tuning the Charge State of (WO3)3 Nanoclusters Deposited on MgO/Ag (001) Films. *J. Phys. Chem. C* **2012**, *116*, 17668−17675.
(41) Shaikhutdinov, S.; Heemeier, M.; Hoffmann, J.; Meusel, I.; Richter, B.; Bäumer, M.; Kuhlenbeck, H.; Libuda, J.; Freund, H. J.; Oldman, R.; et al. Interaction of Oxygen with Palladium Deposited on a Thin Alumina Film. *Surf. Sci.* **2002**, *501*, 270−281.
(42) Yoshitake, M.; Song, W. Fabrication of Epitaxial MIM Structures on NiAl(110) Studied by XPS and Low Energy Electron Diffraction. *Surf. Interface Anal.* **2006**, *38*, 769−772.

DOI: 10.1021/acs.jpcb.7b06790
J. Phys. Chem. B 2018, 122, 788−793